NASA Technical Memorandum 105891

The Effect of Contact Stresses in Four-Point Bend Testing of Graphite/Epoxy and Graphite/PMR–15 Composite Beams

Wieslaw K. Binienda
The University of Akron
Akron, Ohio

Gary D. Roberts
Lewis Research Center
Cleveland, Ohio

and

Demetrios S. Papadopoulos
Case Western Reserve University
Cleveland, Ohio

October 1992

NASA

EFFECT OF CONTACT STRESSES IN FOUR-POINT BEND TESTING OF GRAPHITE/EPOXY AND GRAPHITE/PMR-15 COMPOSITE BEAMS

W.K. Binienda
Civil Engineering Department
The University of Akron
Akron, Ohio 44325-3905

G.D. Roberts
National Aeronautics and Space Administration
Lewis Research Center
Cleveland, Ohio 44135-3191

and

D.S. Papadopoulos
Case Western Reserve University
Cleveland, Ohio 44106

E-7358

ABSTRACT

In this paper, the results of in-plane four-point bend experiments on unidirectionally reinforced composite beams are presented for graphite/epoxy (T300/934) and graphite/polyimide (G30-500/PMR-15) composites. The maximum load and the location of cracks formed during failure were measured for testpieces with fibers oriented at various angles to the beam axis. Since most of the beams failed near one or more of the load points, the strength of the beams was evaluated in terms of a proposed model for the local stress distribution. In this model, an exact solution to the problem of a localized contact force acting on a unidirectionally reinforced half plane is used to describe the local stress field. The stress singularity at the load point is treated in a manner similar to the stress singularity at a crack tip in fracture mechanics problems. Using this approach, the effect of fiber angle and elastic material properties on the strength of the beam is described in terms of a load intensity factor. For fiber angles less than 45° from the beam axis, a single crack is initiated near one of the load points at a critical value of the load intensity factor. The critical load intensity factor decreases with increasing fiber angle. For larger fiber angles, multiple cracks occur at locations both near and away from the load points, and the load intensity factor at failure increases sharply with increasing fiber angle.

1. INTRODUCTION

Beam deflection tests are often used to measure the strength and some of the elastic properties of composite materials. For example, the flexural test is described in ASTM Standard D-790 and the interlaminar short beam shear test is described in ASTM Standard D-2344. Both of these test methods utilize classical beam theory as the basis for data analysis. This type of analysis is strictly applicable only for homogeneous materials. A more detailed analysis of the stress field and the failure mechanism is needed to interpret results of beam tests on composite materials. In spite of this additional complexity, the beam deflection test can be a useful tool for composite materials research. Some advantages of beam tests are that testpieces are easy to prepare, testpieces can be small, grips are not required to hold the testpieces, alignment of the testpieces is very simplified, and strain gauges are not required during testing. These advantages become particularly desirable when a large number of different materials must be tested or a particular material (often an experimental formulation) is available only in small quantities. Also, this kind of experiment is easily adapted for elevated temperature testing and testing under special environmental conditions.

The fatigue and fracture behavior of composites can also be analyzed using three and four-point bend tests. Orange [1] found that initiation and propagation of small cracks in isotropic beams are influenced by contact stresses. In papers by Whitney et al. [2-4] and by Browning et al. [5] the influence of contact stresses in orthotropic beams was shown to be even greater.

Timoshenko [6] has also noted that the stresses under flexure conditions are significantly different from beam theory results, and he offered some of the analytical techniques to account for the contact stresses. Leightniskii [7] obtained the contact stress field for an orthotropic half plane loaded by a concentrated force at the edge. He observed that the stress distribution depends on a ratio of orthotropy (i.e. E_{LL}/E_{TT}, where E_{LL} is the elastic modulus along the fiber direction and E_{TT} is the elastic modulus transverse to fibers) for 0° and 90° fiber angles. Green and Zerna [8] showed the complex potential solution for the general anisotropic case. They presented the stress distributions only for the cases of orthotropic and isotropic materials.

In continuous fiber reinforced composites, the contact stress can be channeled along the fiber axis and affect the stress field at locations far from the load point. This stress channeling phenomenon [9] was analytically and numerically analyzed by Binienda and Saleeb [10] for unidirectionally reinforced composite beams tested under three or four-point bending conditions. They found that both the magnitude and location of the maximum (flexural) tensile stress will be greatly

influenced by the contact stress. This in turn will have a direct bearing on location and propagation of cracks.

In this paper, results of four-point bend tests on unidirectionally reinforced graphite/epoxy and graphite/polyimide beams are reported. The effects of fiber angle and material properties on the breaking load and the location of cracks formed during failure were measured. Experimental results are analyzed using the exact solution to a concentrated force problem from which the local stress conditions at crack initiation are determined.

2. EXPERIMENTAL PROCEDURES

Unidirectional (40 ply) graphite/epoxy and graphite/polyimide laminates were prepared by compression molding. The epoxy laminate was made with Fiberite 1034E prepreg (T300/934) cured for two hours at 350°F. The polyimide laminate was made with Ferro CPI-2237 prepreg (G30-500/PMR-15) cured for two hours at 600°F and postcured for 16 hours at 586°F. The G30-500 fiber was surface treated but not sized. In both cases the fiber volume fraction was 0.6. Typical elastic properties of unidirectional laminates made using these materials are shown in Table 1. The elastic material properties were determined in other experimental programs and were also reported in [11].

Dimensions of both laminates were 6 in. by 12 in. (15.2 cm by 30.4 cm) with the fiber angle along the 12 in. direction. The thickness of the epoxy laminate was about 0.23 in. (.58 cm) and the thickness of the polyimide laminate was about 0.19 in (.48 cm).

Laminates were C-scanned before being cut into smaller testpieces. The C-scan image of the epoxy laminate (Fig. 1a) was uniform without large defects. The C-scan image of the polyimide laminate (Fig. 1b) shows two localized oval defects. Both laminates were cut according to the map shown in Figure 2 using a water-cooled, diamond-impregnated cutting wheel. Hence, four testpieces were prepared for 15, 30, 45, 75, and 90° fiber angles and three testpieces for the 60° fiber angle. No delaminations were observed when testpieces were cut from the epoxy laminate. Delaminations were observed in polyimide testpieces with 60° fiber angle. These testpieces were not used. No other delaminations were observed in the polyimide testpieces, even though some testpieces with fiber angles of 45° and 90° were cut from regions of the laminate in which the C-scan image showed a defect. Widths and thicknesses for epoxy and polyimide testpieces are shown in Tables 2 and 3, respectively.

Four-point bending tests were done using an INSTRON Model 1125 testing machine under displacement control at the rate 0.05 in/min. Forces were measured by a load cell with a maximum range

of 10,000 lbs. The load and displacement signals were recorded on a strip chart recorder.

3. RESULTS AND DISCUSSION

3.1 Beam Tests

In all cases the material responded elastically until the catastrophic failure load was reached. The failure load is shown for each specimen in Tables 2 and 3. In almost all cases the maximum load for graphite/epoxy was about twice that of the graphite/polyimide.

The locations of the cracks are shown for graphite/epoxy composites in Figure 3 and for graphite/polyimide composites in Figure 4. Multiple cracks occurred for graphite/epoxy composites with fiber angles of 90, 75, and 60°. Some of the cracks were located at the load points while others were not. A single crack occurred for fiber angles of 45° and less. For these testpieces, the cracks were initiated at the lower right load point. Polyimide composites failed in a similar manner, except that only a single crack occurred for all fiber angles. For fiber angles of 90, 75, and 45°, the crack usually occurred away from the load points. However a few cracks were located near the upper left load point. For fiber angles of 30 and 15°, the crack was initiated at the lower right load point.

The maximum traction force is defined as the load at failure divided by beam width (beam width equals laminate thickness for these testpieces). The maximum traction force, P/t, is shown in Figure 5 for graphite/epoxy and graphite/polyimide composites. For epoxy beams with fiber angles of 15, 30, and 45°, the traction force decreases with increasing fiber angle, and error bars are relatively small. When the fiber angle is increased from 45 to 60°, the traction force increases and the error bars become larger. The size of the error bars is related to the mode of failure. For low fiber angles, a single crack occurs at the same location for all testpieces, and error bars are small. For high fiber angles, the number and locations of cracks are not the same for different testpieces with the same fiber angle. Because of the different possible failure modes, error bars are large. The change in failure mode and the increase in traction force between 45° and 60° fiber angle indicate that the resistance to local failure at the load points is increasing, so that failure occurs along the bottom of the beam as a result of the bending stress. This type of failure may also be influenced by the stress channeling effect discussed earlier. Results for polyimide composites are similar to those for epoxy composites with three exceptions. First, multiple cracks do not occur in testpieces with high fiber angles. Instead, a single crack occurs away from the load points for all testpieces except one (#4 in Figure 3) with fiber angles of 45° and greater. Second, the failure mode changes from local failure near a load point to

failure along the bottom surface of the beam at a fiber angle of 45° instead of 60°. Third, there is no abrupt increase in the traction force when the failure mode changes. The results for the polyimide composites are somewhat obscured by the lack of data for the 60° fiber angle and the large error bars for the 45° fiber angle. The large error bars for the 45° fiber angle are probably a result of defects in the laminate. As noted earlier, the C-scan image showed an oval shaped defect in the region from which the 45° fiber angle testpieces (identified as #12, 13, 14, and 15 in Figure 2) were cut. Although significant portions of testpieces 14 and 15 lie within the oval region, there were no observable delaminations in these testpieces. Even though there were no observable defects, the failure loads for testpieces 14 and 15 were much lower than those of testpieces 12 and 13 (see Table 3).

For all fiber angles, the traction force is lower for polyimide beams than for epoxy beams. A satisfactory explanation for this difference in strength would require further knowledge of resin, fiber, and interface properties in addition to information about the microscopic failure mechanisms. This type of analysis is beyond the scope of the present work. However, the experimental and analytical techniques developed in this work are now being used in further studies which include a closer examination of the microscopic failure mechanisms and the effect of matrix, fiber, and interface properties on the strength of graphite/polyimide composites.

Since failure in many of the testpieces occurs as a result of local stresses near a load point, it is misleading to describe the strength of these beams only in terms of the traction force at failure shown in Figure 5. An analysis of the local stress field near a load point is presented below. The data presented above are then re-examined in terms of the local stress analysis.

3.2. Analysis of Contact Stresses

The problem of a concentrated force applied to an anisotropic half space was formulated and solved by Binienda et al. [10] using the Fourier integral technique proposed by Lekhnitskii [7] for plane strain elasto-static conditions.

Consider an anisotropic half plane loaded as in Figure 6. The governing equation in x-y coordinate system in terms of Airy stress function F(x,y) is:

$$b_{22}\frac{\partial^4 F}{\partial x^4} - 2b_{26}\frac{\partial^4 F}{\partial x^3 \partial y} + (2b_{12}+b_{66})\frac{\partial^4 F}{\partial x^2 \partial y^2} - 2b_{16}\frac{\partial^4 F}{\partial x \partial y^3} + b_{11}\frac{\partial^4 F}{\partial y^4} = 0 \qquad (1)$$

where

$$\left.\begin{aligned}
b_{11} &= a_{11}\cos^4\theta + (2a_{12}+a_{66})\sin^2\theta\cos^2\theta + a_{22}\sin^4\theta \\
b_{22} &= a_{11}\sin^4\theta + (2a_{12}+a_{66})\sin^2\theta\cos^2\theta + a_{22}\cos^4\theta \\
b_{12} &= a_{12} + (a_{11} + a_{22} - 2a_{12} - a_{66})\sin^2\theta\cos^2\theta \\
b_{66} &= a_{66} + 4(a_{11} + a_{22} - 2a_{12} - a_{66})\sin^2\theta\cos^2\theta \\
b_{16} &= [a_{22}\sin^2\theta - a_{11}\cos^2\theta + \tfrac{1}{2}(2a_{12}+a_{66})\cos 2\theta]\sin 2\theta \\
b_{26} &= [a_{22}\cos^2\theta - a_{11}\sin^2\theta - \tfrac{1}{2}(2a_{12}+a_{66})\cos 2\theta]\sin 2\theta
\end{aligned}\right\} \qquad (2)$$

and

$$a_{11} = \frac{1}{E_{LL}}; \qquad a_{22} = \frac{1}{E_{TT}}; \qquad a_{12} = -\frac{\nu_{LT}}{E_{LL}}; \qquad a_{66} = \frac{1}{G_{LT}} \qquad (3)$$

The Hookes's law in this case is:

$$\left.\begin{aligned}
\epsilon_{xx} &= b_{11}\sigma_{xx} + b_{12}\sigma_{yy} + b_{16}\sigma_{xy} \\
\epsilon_{xx} &= b_{12}\sigma_{xx} + b_{22}\sigma_{yy} + b_{26}\sigma_{xy} \\
\epsilon_{xx} &= b_{16}\sigma_{xx} + b_{26}\sigma_{yy} + b_{66}\sigma_{xy}
\end{aligned}\right\} \qquad (4)$$

The boundary conditions are given in the following form:

$$\left.\begin{aligned}
&\text{for } y = 0 && \sigma_{yy} = -N(x) = -\frac{P}{2\epsilon} && \text{for } |x| < \epsilon \\
&\text{for } y = 0 && \sigma_{yy} = 0 && \text{for } |x| \geq \epsilon \\
&\text{for } y = 0 && \sigma_{xy} = 0 && \text{for } -\infty < x < \infty \\
&\text{for } x^2 + y^2 = \infty && \sigma_{xx} = \sigma_{yy} = \sigma_{xy} = 0 &&
\end{aligned}\right\} \qquad (5)$$

Using the Fourier transformation concept the stress function may be expressed as:

$$F(x,y) = \frac{1}{2\pi} \int_{-\infty}^{\infty} \phi(s,y)\, e^{-isx}\, ds \tag{6}$$

Upon differentiation of Eq. (6) and substitution of the appropriate results into the Eq. (1) the particular solution to the governing equation can easily be found as:

$$\phi(s,y) = C(s)\, e^{rsy} \tag{7}$$

giving the characteristic equation:

$$r^4 + 2i\frac{b_{16}}{b_{11}} r^3 - \frac{2b_{12}+b_{66}}{b_{11}} r^2 - 2i\frac{b_{26}}{b_{11}} r + \frac{b_{22}}{b_{11}} = 0 \tag{8}$$

that has four complex roots in the following form:

$$\left.\begin{array}{ll} r_1 = a + ib & r_2 = c + id \\ r_3 = -a + ib & r_4 = -c + id \end{array}\right\} \tag{9}$$

where a,b,c,d are real constants related to material properties of the composite and $a,c > 0$ $(i = \sqrt{-1})$.

The stress function (6) obtained using four particular solutions for each r_k (9) that satisfy the boundary conditions gives the equation for stresses (the details of the derivation one may find in [10]):

$$\sigma_{xx}(x,y) = \frac{Pix}{2\pi}\left[\frac{r_1 r_2}{(r_1 y - ix)(r_2 y - ix)} - \frac{r_3 r_4}{(r_3 y - ix)(r_4 y - ix)}\right] \tag{10}$$

$$\sigma_{yy}(x,y) = \frac{-P}{2\pi}\left[\frac{(r_1 + r_2)y - ix}{(r_1 y - ix)(r_2 y - ix)} - \frac{(r_3 + r_4)y - ix}{(r_3 y - ix)(r_4 y - ix)}\right] \tag{11}$$

$$\sigma_{xy}(x,y) = \frac{Piy}{2\pi}\left[\frac{r_1 r_2}{(r_1 y - ix)(r_2 y - ix)} - \frac{r_3 r_4}{(r_3 y - ix)(r_4 y - ix)}\right] \tag{12}$$

In polar coordinates r,φ (see Fig. 7) it can be easily shown that $\sigma_{\varphi\varphi} = \sigma_{R\varphi} = 0$ while the only non zero radial stress is:

$$\sigma_{RR} = \frac{P}{\pi R}\,\mathbf{M}(a,b,c,d,\varphi) \tag{13}$$

where $\mathbf{M}(a,b,c,d,\varphi)$ is a material related parameter that can be expressed by a,b,c,d and polar coordinate φ as follows:

$$\mathbf{M} = \frac{-4\{\sin\varphi[(a^2+b^2)c+(c^2+d^2)a]-\cos\varphi(bc+ad)\}}{[1+a^2+b^2+\cos2\varphi(1-a^2-b^2)-2b\sin2\varphi]\,[1+c^2+d^2-\cos2\varphi(a^2+b^2-1)-2d\sin2\varphi]} \tag{14}$$

The orthotropic case (i.e. $\theta = 0^o$ or 90^o) can be easily obtained by noting that the imaginary part of the roots of the characteristic equation is zero (i.e. b = d = 0). Then the radial stress become:

$$\sigma_{rr}(x,y) = -\frac{P\,a\,c\,(a+c)}{\pi R(a^2\sin^2\varphi+\cos^2\varphi)(c^2\sin^2\varphi+\cos^2\varphi)}\sin\varphi \tag{15}$$

In case of isotropic material it can be shown that a=c=1 and $\mathbf{M} = -2\sin\varphi$. Therefore, the radial stress takes well known form:

$$\sigma_{RR} = -\frac{2P}{\pi}\,\frac{\sin\varphi}{R} \tag{16}$$

In the Eq. (13) the denominator πR constitutes the order of the singularity -1 which is true for all concentrated load problems. The numerator P $\mathbf{M}$, is similar to the stress intensity factor, k, for the crack problem. For the case of unit load the parameter $\mathbf{M}$ depends only on the fiber geometry and material properties. Similarly, k depends only on the geometry and configuration of the cracks and the material properties. Therefore, the parameter $\mathbf{M}$ can be called a normalized load intensity factor with respect to the applied concentrated load.

3.3. Analysis of Experimental Data

Based on the discussion in the previous section, the intensity of the local stress field is represented by $\pi R(\sigma_{RR})$. According to Equation 13, the value of $\pi R(\sigma_{RR})$ at the instant of failure can be calculated by multiplying the experimentally determined traction force at failure (P/t from Figure 5) by the appropriate value of the normalized load intensity factor (M from Figure 8 or 9). If a stress criterion for failure is valid for these materials, this product could represent a "critical load intensity factor" analogous to the critical stress intensity factor used in fracture mechanics. One difficulty in using this approach for composite materials is that the dependence of σ_{RR} on ϕ is much more complex for composites (see Equations 13 and 14) than for a homogeneous material (see Equation 16). For composites it is not possible to remove the ϕ dependence from the load intensity factor by writing M in the form of $M(\Theta,\phi)=g(\Theta)h(\phi)$. As a result, some value of ϕ must be chosen in order to calculate the load intensity factor. Results are shown in Figure 10 for the case of $\phi=(180^{\circ}-\Theta)$. This value of ϕ was chosen because the absolute value of M has a maximum near this value of ϕ, and most of the cracks appear to begin at the load point and travel along the fiber direction. The data in Figure 10 indicate that the local (compressive) stress at failure is highest for high fiber angles, even though the traction force (shown in Figure 5) is not. Since failure at high fiber angles involves both local stresses and bending stresses, the load intensity factors shown in Figure 10 are not critical values for local failure. For low fiber angles, failure always occurs at the lower right load point. Since the bending stress is zero at this load point, the load intensity factors shown in Figure 10 could be critical values. However, further testing is needed to determine the validity of using the critical load intensity factor as a general criterion for failure in this type of four-point bend test.

4. CONCLUSIONS

Since most of the composite beams failed as a result of cracks initiated at one or more of the load points, some form of local stress analysis is required to interpret the test data. The intensity of the local stress field can be easily calculated using the analytical method proposed in this paper. Although the results presented in this paper demonstrate that this method provides useful information about the resistance of composites to local failure, the validity of this approach needs to be further demonstrated. In particular, the idea that failure occurs at a critical value of the load intensity factor needs to be demonstrated by testing of beams with the same fiber angle but different dimensions. The effect of test parameters, such as the diameter of the loading pins, also needs to be examined. Finite element modeling of the local stress distribution along with microscopic examination of crack initiation under incremental loading would also be useful.

REFERENCES

[1] Orange, T.W., "Stress intensity and Crack Displacement for Small Edge Crack", NASA Technical Paper 2801, 1988.

[2] Whitney, J.M., "Elasticity Analysis of Orthotropic Beams Under Concentrated Loads", Composite Science and Technology, Vol 22 pp.167-183, 1985.

[3] Whitney, J.M. and Browning, C.E., "On Short-Beam Shear Tests for Composite Materials", Experimental Mechanics Vol. 25, pp.294-300, 1985.

[4] Whitney, J.M. and Browning, C.E., "Materials Characterization for Matrix Dominated Failure Modes" in Effects of Defects in Composite Materials, ASTM STP 836 (ed. D.J. Wilkins), pp. 104-124, 1984.

[5] Browning, C.E., Abrams, F.L. and Whitney, J.M., "A Four-Point Shear Test for Graphite/Epoxy Composites" in Composite Materials: Quality Assurance and Processing, ASTM STP 797 (ed. C. E. Browning), pp.54-74, 1983.

[6] Timoshenko, S. and Goodier, J.N., "Theory of Elasticity" secon ed. McGraw Hill, Chapter 4.

[7] Lekhnitskii, S.G, "Anisotropic Plates", Gordon and Breach Science Publishers, 1968, Chapter 4.

[8] Green, A.E. and Zerna, W., "Theoretical Elasticity", 2-nd edition, Oxford, 1968.

[9] Everstine, G.C. and Pipkin, A.C., "Stress Channeling in Transversely Isotropic Elastic Composites", J. Appl. Math. Phys. (ZAMP), Vol. 22, pp. 825-834, 1971.

[10] Binienda, W.K. and Saleeb A.F., "The Effect of Contact Stresses in Predicting Location of Crack Initiation ib Short Unidirectionally-Reinforced Composite Beams", submitted to European Journal of Mechanics, January 1992.

[11] Irvine, T.B. and Ginty C.A., "Progressive Fracture of Fiber Composites", NASA TM 83701, October 1983

Table 1.

Elastic Properties of Composites

Materials	E_{LL} GPa (Msi)	E_{TT} GPa (Msi)	G_{LT} GPa (Msi)	ν_{LT}
Graphite/Epoxy (T300/934)	140 (20)	10.3 (1.50)	6.6 (0.95)	0.21
Graphite/Polyimide (G30-500/PMR-15)	150 (22)	8.4 (1.23)	4.0 (0.58)	0.27

Table 2

Failure Loads And Dimensions For Graphite/Epoxy Composites

Specimen	Angle Degrees	Load P (N)	Width (mm)	Thickness t (mm)	P/t (N/mm)	Average P/t (N/mm)	Std. Dev (N/mm)
1	90	4114.6	15.65	5.85	703.4		
2	90	6449.9	16.03	5.79	1114.0	1075.5	221.3
3	90	7152.7	16.07	5.81	1231.1		
4	90	7295.1	16.06	5.82	1253.5		
5	75	6641.2	15.68	5.83	1139.1		
6	75	8380.5	16.03	5.82	1439.9	1320.2	118.0
7	75	8198.1	16.03	5.82	1408.6		
8	75	7526.4	16.04	5.82	1293.2		
9	60	9296.8	16.03	5.84	1591.9		
10	60	9341.3	16.02	5.86	1594.1	1479.1	161.1
11	60	7295.1	15.61	5.83	1251.3		
12	45	6316.5	16.02	5.80	1089.0		
13	45	6828.0	16.02	5.79	1179.3	1146.0	40.5
14	45	6761.3	16.04	5.78	1169.8		
15	45	*	16.25	5.78	*		
16	30	7206.1	16.05	5.88	1225.5		
17	30	7406.3	16.01	5.86	1263.9	1283.1	48.3
18	30	7517.5	16.01	5.85	1285.0		
19	30	7917.8	15.68	5.83	1358.1		
20	15	9474.7	16.02	5.86	1616.8		
21	15	9608.2	16.02	5.86	1639.6	1654.0	31.7
22	15	9706.0	16.02	5.86	1656.3		
23	15	9964.0	16.02	5.85	1703.3		

Table 3

Failure Loads And Dimensions For Graphite/Polyimide Composites

Specimen	Angle Degrees	Load P (N)	Width (mm)	Thickness t (mm)	P/t (N/mm)	Average P/t (N/mm)	Std. Dev. (N/mm)
1	90	2037.3	16.01	4.92	414.1		
2	90	2397.6	16.03	4.85	494.4	452.4	35.8
3	90	2339.8	16.04	4.86	481.4		
4	90	2023.9	15.67	4.82	419.9		
5	75	2273.0	15.65	4.87	466.7		
6	75	2713.4	16.00	4.86	558.3	523.0	34.0
7	75	2580.0	16.02	4.84	533.1		
8	75	2584.4	16.04	4.84	534.0		
12	45	3747.6	15.98	4.88	768.0		
13	45	3465.2	16.01	4.85	714.5	588.1	16.3
14	45	2620.0	16.03	4.85	540.2		
15	45	1596.9	16.05	4.84	329.9		
16	30	3936.7	16.01	4.88	806.7		
17	30	3549.7	16.01	4.89	725.9	767.3	33.5
18	30	3870.0	16.02	4.88	793.0		
19	30	3620.9	16.02	4.87	743.5		
20	15	5426.8	16.01	4.90	1107.5		
21	15	5159.9	15.99	4.87	1059.5	1067.8	43.1
22	15	5373.5	15.99	4.87	1103.4		
23	15	4893.0	15.99	4.89	1000.6		

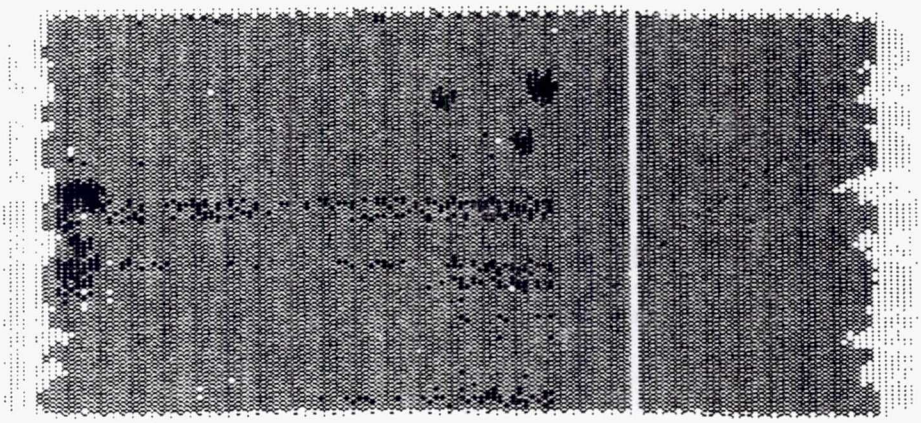

(a) Graphite/Epoxy

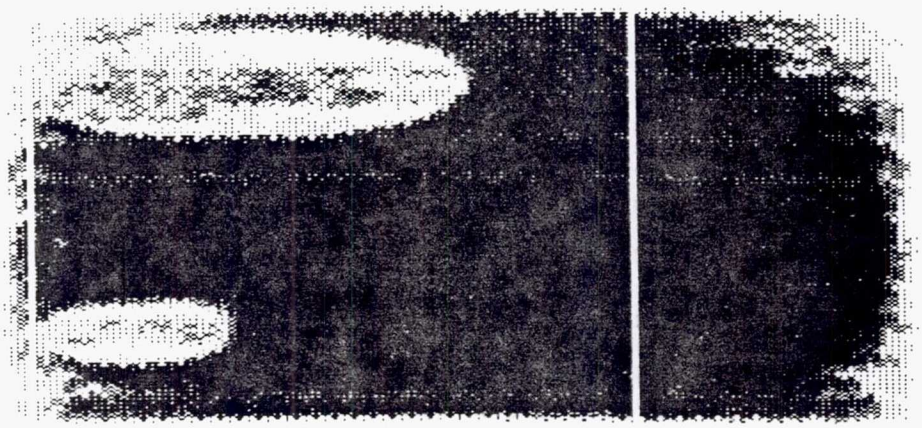

(b) Graphite/Polyimide

Figure 1. C-scan images of (a) graphite/epoxy and (b) graphite/polyimide composites.

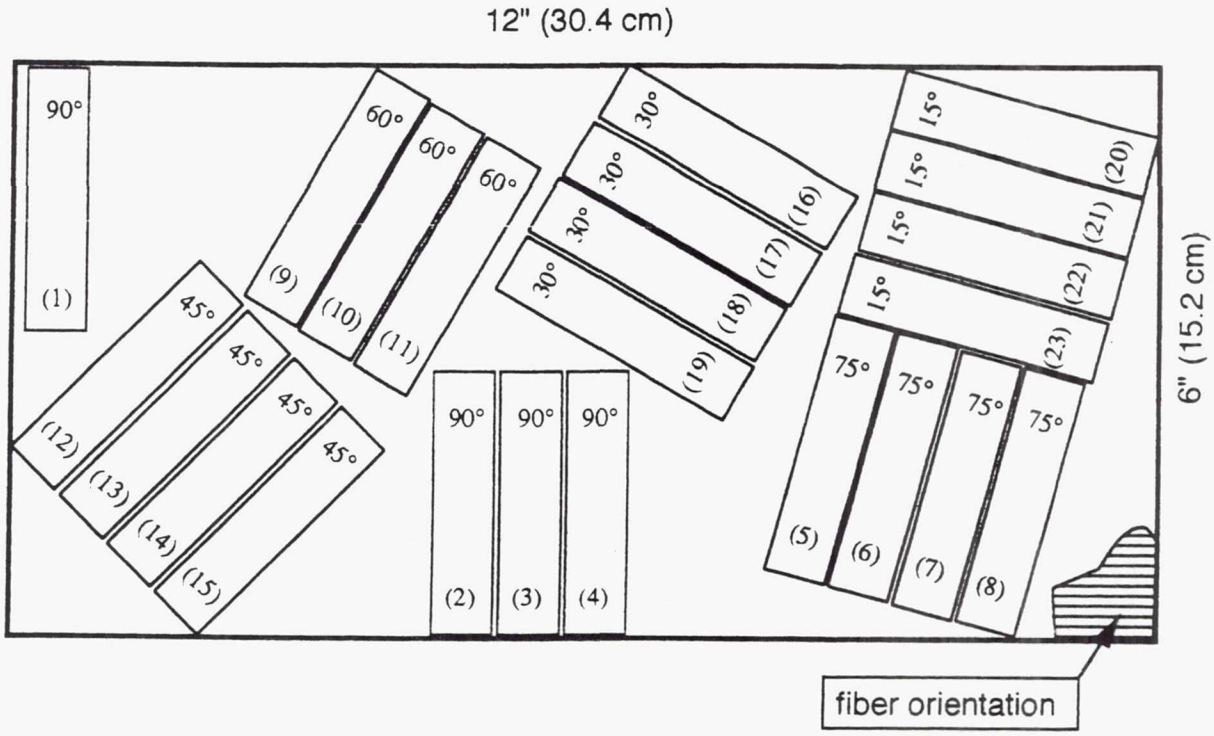

Figure 2. Locations of testpieces cut from 6"×12" laminates. Fiber angles relative to beam axis and testpiece identification numbers are indicated for each testpiece.

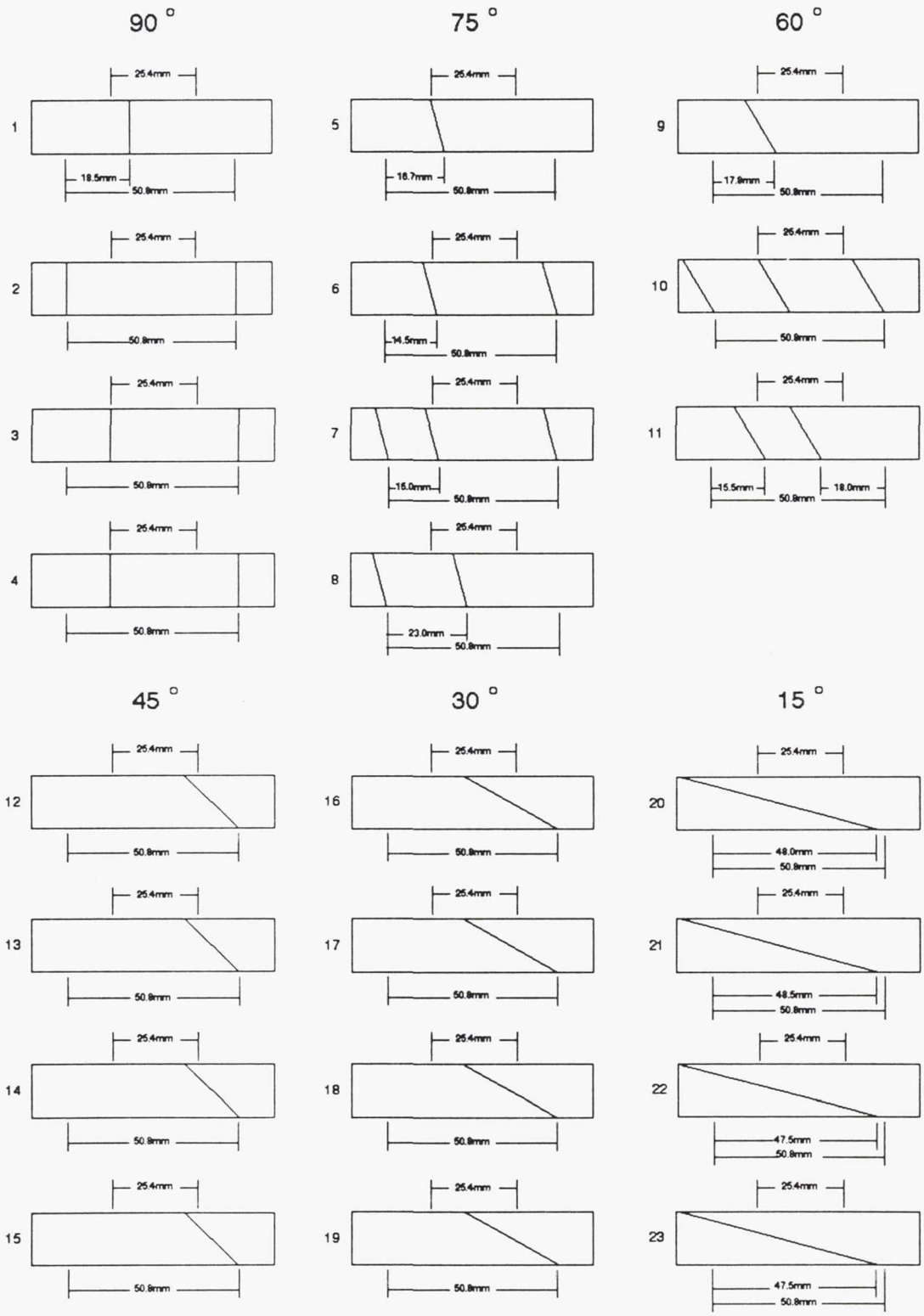

Figure 3. Failure locations in graphite/epoxy beams.

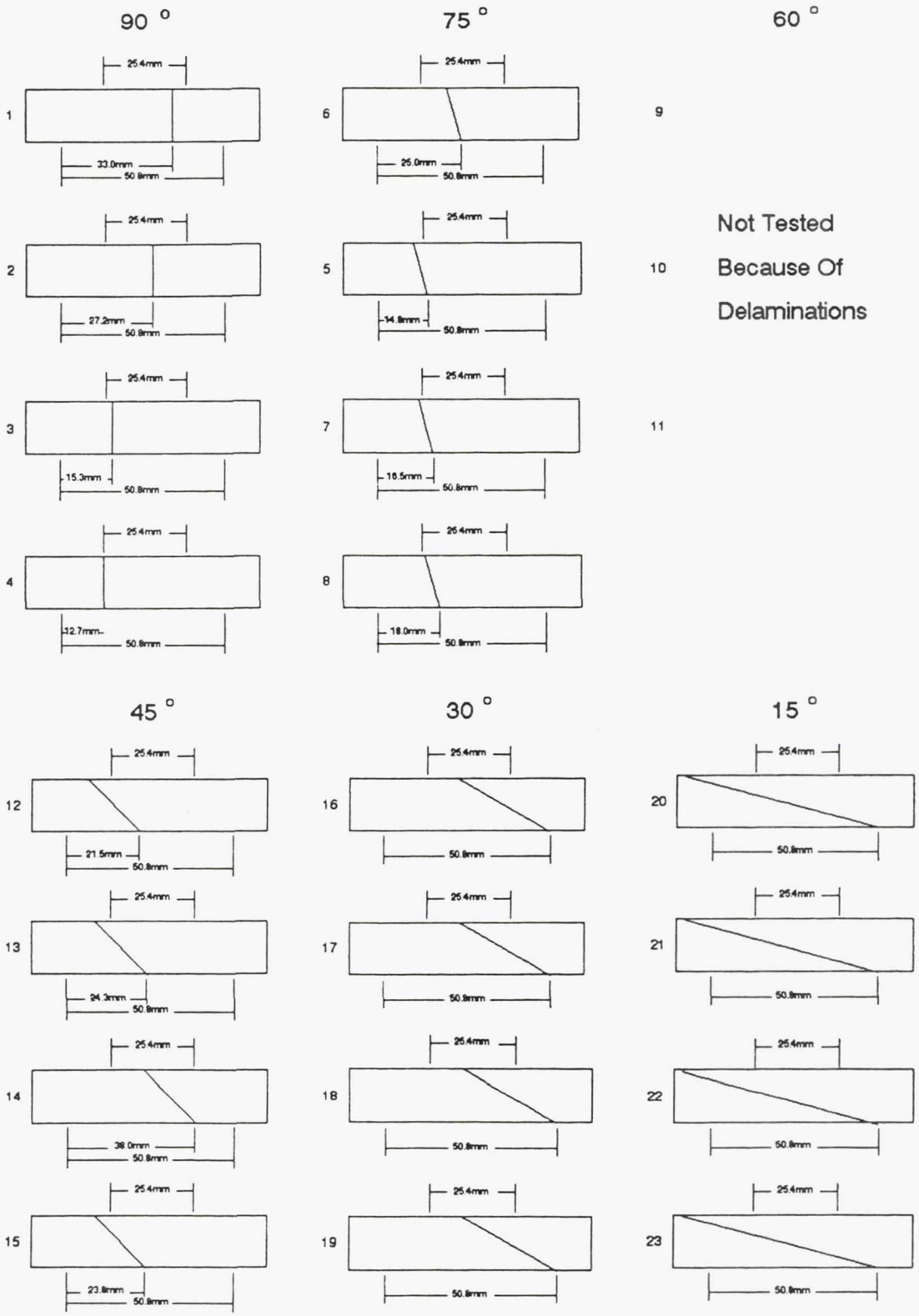

Figure 4. Failure locations in graphite/polyimide beams.

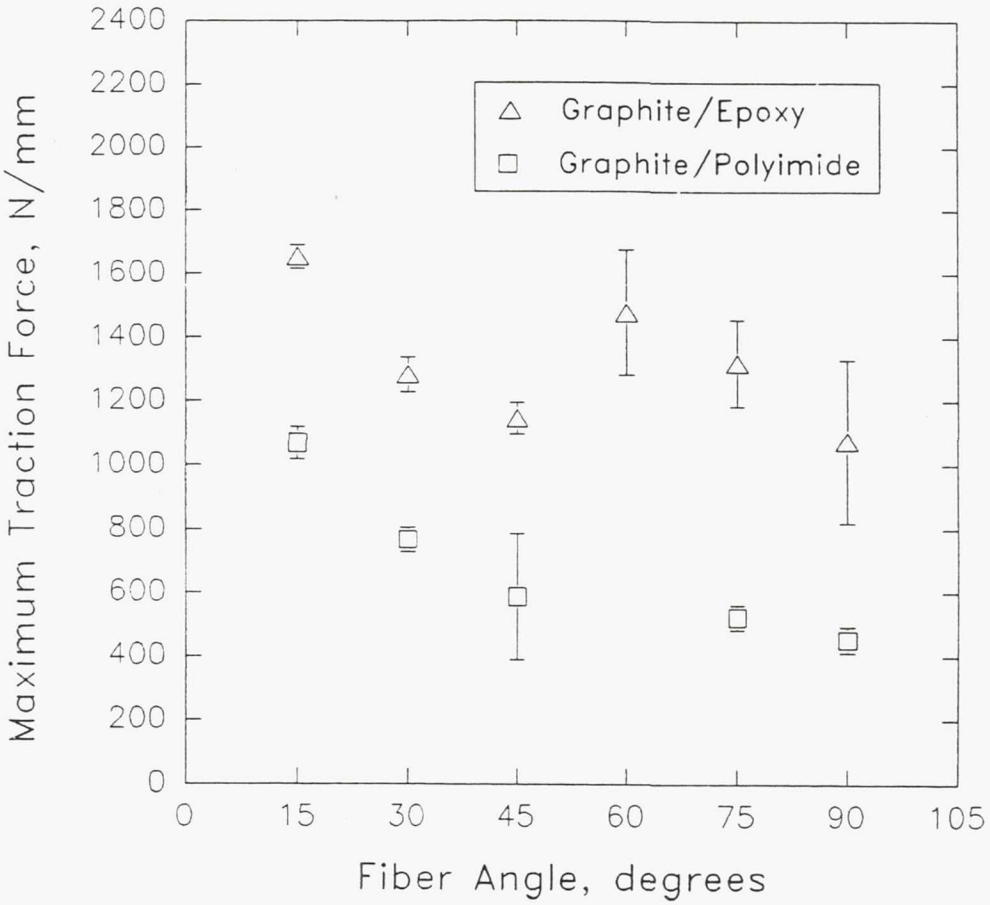

Figure 5. Maximum traction force versus fiber angle for graphite/epoxy and graphite/polyimide composites. Error bars are shown for 95% confidence interval.

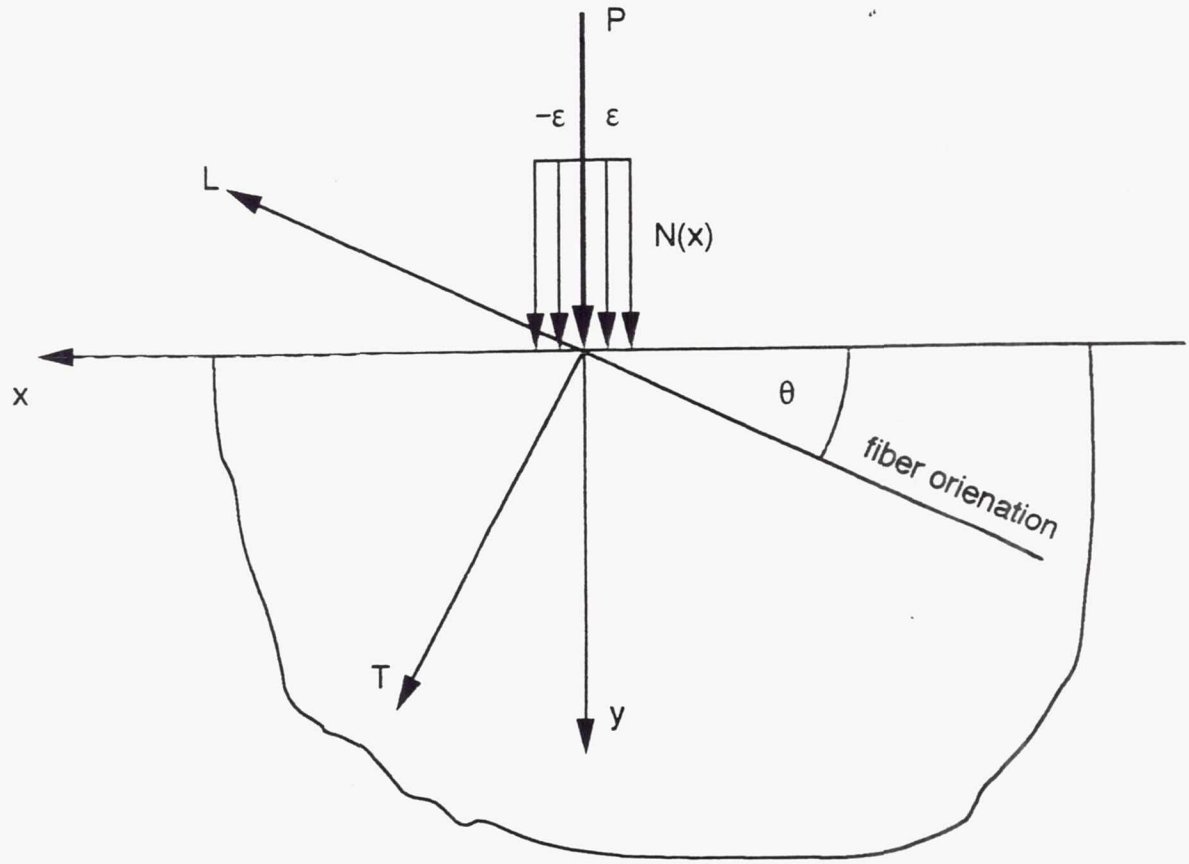

Figure 6. The anisotropic half-plane problem. (See text)

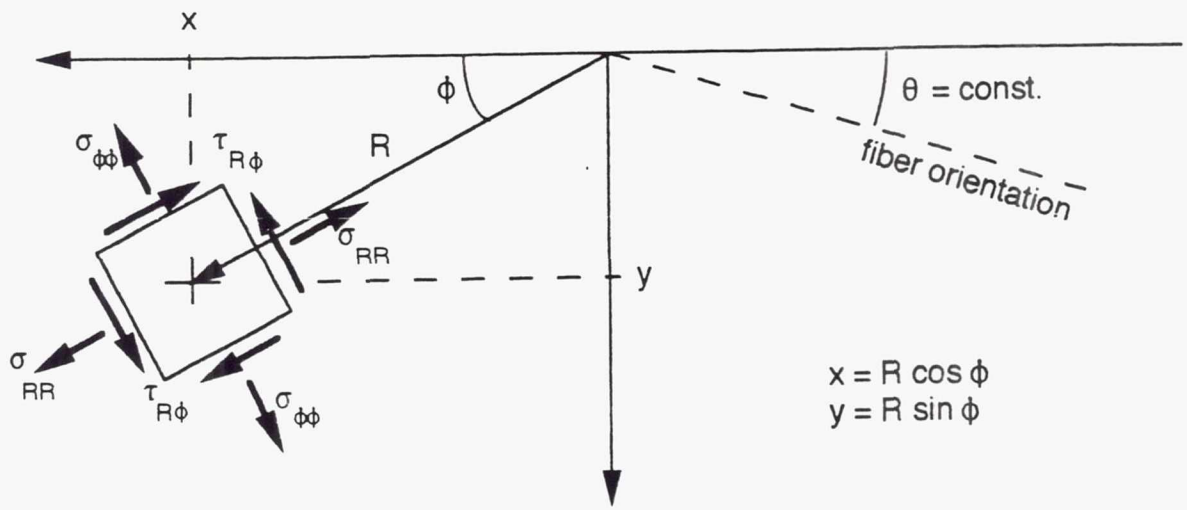

Figure 7. Cartesian/polar coordinate transformation.

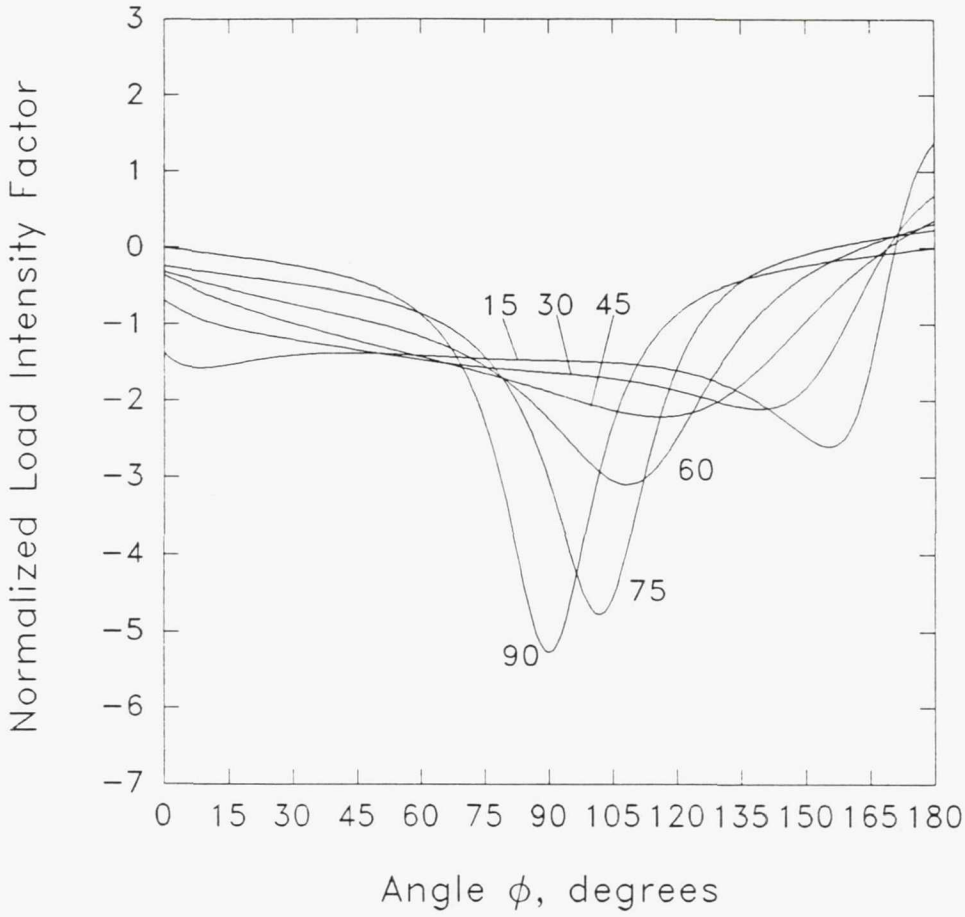

Figure 8. Normalized load intensity factors for graphite/epoxy composites. Fiber angle is indicated for each curve.

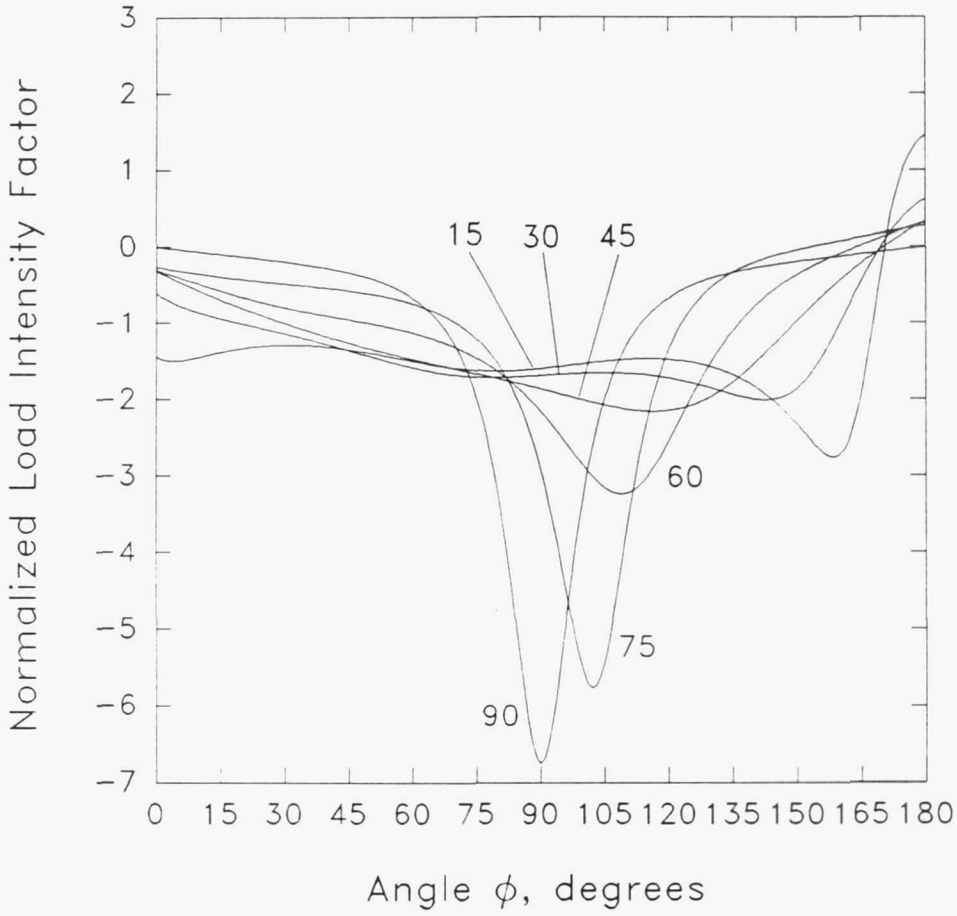

Figure 9. Normalized load intensity factors for graphite/polyimide composites. Fiber angle is indicated for each curve.

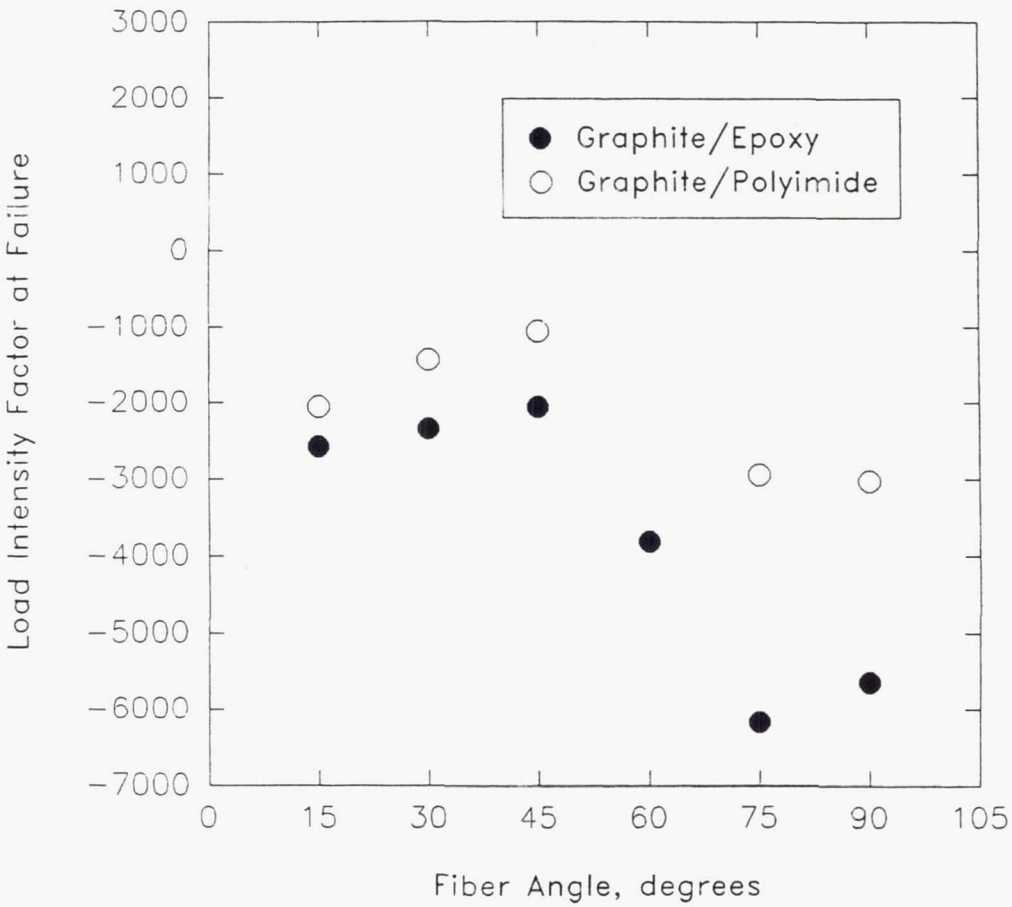

Figure 10. Load intensity factors at failure for graphite/epoxy and graphite/polyimide composites.

REPORT DOCUMENTATION PAGE

Form Approved
OMB No. 0704-0188

1. AGENCY USE ONLY (*Leave blank*)	2. REPORT DATE	3. REPORT TYPE AND DATES COVERED
	October 1992	Technical Memorandum

4. TITLE AND SUBTITLE

The Effect of Contact Stresses in Four-Point Bend Testing of Graphite/Epoxy and Graphite/PMR–15 Composite Beams

5. FUNDING NUMBERS

WU–505–63–5A

6. AUTHOR(S)

Wieslaw K. Binienda, Gary D. Roberts, and Demetrios S. Papadopoulos

7. PERFORMING ORGANIZATION NAME(S) AND ADDRESS(ES)

National Aeronautics and Space Administration
Lewis Research Center
Cleveland, Ohio 44135–3191

8. PERFORMING ORGANIZATION REPORT NUMBER

E–7358

9. SPONSORING/MONITORING AGENCY NAMES(S) AND ADDRESS(ES)

National Aeronautics and Space Administration
Washington, D.C. 20546–0001

10. SPONSORING/MONITORING AGENCY REPORT NUMBER

NASA TM–105891

11. SUPPLEMENTARY NOTES

Wieslaw K. Binienda, The University of Akron, Department of Civil Engineering, Akron, Ohio 44325–3905, Gary D. Roberts, NASA Lewis Research Center, Cleveland, Ohio and Demetrios S. Papadopoulos, Case Western Reserve University, Cleveland, Ohio 44106. Responsible person, Gary D. Roberts, (216) 433–3244.

12a. DISTRIBUTION/AVAILABILITY STATEMENT

Unclassified - Unlimited
Subject Category 24

12b. DISTRIBUTION CODE

13. ABSTRACT ***(Maximum 200 words)***

In this paper, the results of in-plane four-point bend experiments on unidirectionally reinforced composite beams are presented for graphite/epoxy (T300/934) and graphite/polyimide (G30–500/PMR–15) composites. The maximum load and the location of cracks formed during failure were measured for testpieces with fibers oriented at various angles to the beam axis. Since most of the beams failed near one or more of the load points, the strength of the beams was evaluated in terms of a proposed model for the local stress distribution. In this model, an exact solution to the problem of a localized contact force acting on a unidirectionally reinforced half plane is used to describe the local stress field. The stress singularity at the load point is treated in a manner similar to the stress singularity at a crack tip in fracture mechanics problems. Using this approach, the effect of fiber angle and elastic material properties on the strength of the beam is described in terms of a load intensity factor. For fiber angles less than 45° from the beam axis, a single crack is initiated near one of the load points at a critical value of the load intensity factor. The critical load intensity factor decreases with increasing fiber angle. For larger fiber angles, multiple cracks occur at locations both near and away from the load points, and the load intensity factor at failure increases sharply with increasing fiber angle.

14. SUBJECT TERMS

Composite materials; Polymer matrix composites; Bend tests; Mechanical properties

15. NUMBER OF PAGES
24

16. PRICE CODE
A03

17. SECURITY CLASSIFICATION OF REPORT	18. SECURITY CLASSIFICATION OF THIS PAGE	19. SECURITY CLASSIFICATION OF ABSTRACT	20. LIMITATION OF ABSTRACT
Unclassified	Unclassified	Unclassified	

National Aeronautics and
Space Administration

Lewis Research Center
Cleveland, Ohio 44135

FOURTH CLASS MAIL

ADDRESS CORRECTION REQUESTED

Official Business
Penalty for Private Use $300

Postage and Fees Paid
National Aeronautics and
Space Administration
NASA 451